

SIMULATION OF PHOSPHORUS IMPLANTATION INTO SILICON WITH A SINGLE PARAMETER ELECTRONIC STOPPING POWER MODEL

DAVID CAI*

Theoretical Division, Los Alamos National Laboratory, Los Alamos, NM 87545, USA

CHARLES M. SNELL

*Applied Theoretical and Computational Physics Division, Los Alamos National Laboratory,
Los Alamos, NM 87545, USA*

KEITH M. BEARDMORE and NIELS GRØNBECHE-JENSEN

Theoretical Division, Los Alamos National Laboratory, Los Alamos, NM 87545, USA

Received 3 October 1997

Revised 19 March 1998

We simulate dopant profiles for phosphorus implantation into silicon using a new model for electronic stopping power. In this model, the electronic stopping power is factorized into a globally averaged effective charge Z_1^* , and a local charge density dependent electronic stopping power for a proton. There is only a single adjustable parameter in the model, namely the one electron radius r_s^0 which controls Z_1^* . By fine tuning this parameter, we obtain excellent agreement between simulated dopant profiles and the SIMS data over a wide range of energies for the channeling case. Our work provides a further example of implant species, in addition to boron and arsenic, to verify the validity of the electronic stopping power model and to illustrate its generality for studies of physical processes involving electronic stopping.

1. Introduction

Monte Carlo and molecular dynamics simulations of ion trajectories in a target material require a good description of the physics of electronic stopping in the high energy regime. The issue of the electronic stopping power is especially important when the target is crystalline and ions can propagate along preferred channel directions in the lattice. For this case, electronic stopping becomes a dominant factor in determining final stopping ranges of the channeling ions. As is well known, the classic Lindhard-Scharff-Schiott theory¹ is applicable only to amorphous materials and underestimates electronic stopping along channeling directions. It thus tends to give an excessively high estimate of the energy threshold below which electronic stopping effects can safely be neglected when modeling ion implantation into crystalline materials. For the channeling case, a good understanding of electronic stopping is essential because the distribution of stopping ranges of ions can still be significantly affected by the electronic stopping power even at relatively low energies.

*Present Address: Courant Institute of Mathematical Sciences, New York, NY 10012, USA

Recently we proposed a model for electronic stopping power for ion implantation modeling.² Based on the spirit of the Brandt-Kitagawa (BK) effective charge theory,³ it models the electronic stopping power for an ion in terms of two factors: (i) a globally averaged effective charge taking into account effects of close and distant collisions by target electrons with the ion, and (ii) a local charge density dependent electronic stopping power for a proton. This model was implemented into both molecular dynamics and Monte Carlo simulations. The results of the dopant profile simulation for both boron and arsenic implants into crystalline and amorphous silicon have demonstrated that our model can successfully capture the *physics* of electronic stopping in ion implantation over a wide range of energies. The model is phenomenologically economical, i.e., it has only one tuning parameter, namely an averaged one electron radius r_s^0 which controls the effective charge of the ion. A single numerical value of this parameter was used for the simulation of both boron and arsenic implantation. Good agreement of dopant profiles with experimental profiles measured by secondary-ion mass spectroscopy (SIMS) was achieved for both species with this single r_s^0 numerical value.

We note that the BK theory uses a statistical model for the partially ionized projectile and does not account for shell structure. Therefore, it can only provide an averaged description of electronic stopping power as a function of the projectile atomic number Z_1 .⁴ The experimentally observed Z_1 oscillations in electronic stopping are a complex phenomenon, attributable to the electronic shell structures of both the incident ion and the target atom.^{5,6,7,8,9} On account of the dependence of the Z_1 oscillation on both the ion and target material, we expect that the parameter r_s^0 can be tuned to different numerical values for different combinations of implant species and substrate material. This fine tuning can be viewed as a phenomenological procedure to incorporate the physics of Z_1 oscillations. In the present work, we will verify this phenomenological approach for phosphorus implantation into silicon and show that our electronic stopping power can successfully model channeling of phosphorus implants into single-crystal silicon, thus extending our electronic stopping power model to the case of phosphorus-on-silicon implants. This further illustrates the potential wide applicability of the model in studies of physical processes that involve electronic stopping.

The paper is organized as follows. In Sec. 2 we summarize the main features of our electronic stopping power model and briefly compare it with other models that have been used in various Monte Carlo simulations. Atomic units $e = \hbar = m_e = 1$ are used in the description of our model. In Sec. 3 we describe the implementation of our model into a MARLOWE platform,¹⁰ and into a molecular dynamics (MD) based implant simulator.¹¹ We then present a comparison between our simulation results and SIMS data for phosphorus implantation into silicon. In Sec. 4 we make concluding remarks.

2. The Model

In our model,² based on an effective charge scaling argument, the electronic stopping power of an ion can be factorized into two components. One is the effective charge Z_1^* of the ion of velocity v_1 , which can be expressed as

$$Z_1^* = Z_1 \gamma(v_1, r_s^0), \quad (1)$$

where Z_1 is the atomic number of the ion and $\gamma(v_1, r_s^0)$ is the fractional effective charge of the ion. The second is the charge density dependent electronic stopping power for a proton $S_p(v_1, r_s)$. Here r_s is the one electron radius, $r_s = [3/(4\pi\rho(\mathbf{x}))]^{1/3}$, where $\rho(\mathbf{x})$ is the charge density of the target. In our treatment $\gamma(v_1, r_s^0)$ does not depend on the local charge density, instead, it is controlled by the parameter r_s^0 , which is the only adjustable parameter in the model.

After taking account of the energy loss of the ion in soft, distant collisions with target electrons and the energy loss in hard close collisions, the BK analysis gives the fractional effective charge

$$\gamma(v_1, r_s^0) = q(v_1, r_s^0) + C[1 - q(v_1, r_s^0)] \ln \left[1 + \left(\frac{4\Lambda(v_1, r_s^0)}{r_s^0} \right)^2 \right]. \quad (2)$$

Here C is weakly dependent on the target and has a numerical value of about 1/2. Below, it is set to be one-half. The ion size parameter $\Lambda(v_1, r_s^0)$ is

$$\Lambda(v_1, r_s^0) = \frac{2a_0[1 - q(v_1, r_s^0)]^{2/3}}{Z_1^{1/3}[1 - (1 - q(v_1, r_s^0))/7]}, \quad (3)$$

which is used in the statistical model to describe the partially ionized projectile. Here $a_0 = 0.24005$ and the ionization fraction $q(v_1, r_s^0)$ obeys the following scaling

$$q(v_1, r_s^0) = 1 - \exp[-0.95(y_r(v_1, r_s^0) - 0.07)]. \quad (4)$$

This scaling was condensed from extensive experimental data for ions $3 \leq Z_1 \leq 92$.¹² The reduced relative velocity $y_r(v_1, r_s^0)$ is defined as

$$y_r(v_1, r_s^0) = \frac{v_r(v_1, r_s^0)}{v_B Z_1^{2/3}}, \quad (5)$$

where v_B is the Bohr velocity. Underlying Eq. (4) is the stripping criterion that the electrons of the ion which have an orbital velocity lower than the relative velocity between the ion and the electrons in the medium are stripped off. Averaging relative velocity over the conduction electrons leads to:¹³

$$v_r(v_1, r_s^0) = v_1 \left(1 + \frac{v_F^2}{5v_1^2} \right) \quad \text{for } v_1 \geq v_F \quad (6)$$

$$v_r(v_1, r_s^0) = \frac{3v_F}{4} \left(1 + \frac{2v_1^2}{3v_F^2} - \frac{v_1^4}{15v_F^4} \right) \quad \text{for } v_1 < v_F \quad (7)$$

In our model,² the Fermi velocity is related to r_s^0 : $v_F = 1/(\alpha r_s^0)$, $\alpha = [4/(9\pi)]^{1/3}$.

The electronic stopping power for a proton in our model uses results derived from a nonlinear density-functional formalism:¹⁴

$$S_p(v_1, r_s) = - \left(\frac{dE}{dx} \right)_R G(r_s), \quad (8)$$

where

$$\left(\frac{dE}{dx} \right)_R = \frac{2v_1}{3\pi} \left[\ln \left(1 + \frac{\pi}{\alpha r_s} \right) - \frac{1}{1 + \alpha r_s/\pi} \right] \quad (9)$$

is the Ritchie formula for the energy loss per unit path length of a proton moving at velocity v_1 in the electron gas derived from a linear response theory. The correction factor $G(r_s)$ is a computationally convenient way to incorporate the density-functional results and it has the following form

$$G(r_s) = 1.00 + 0.717r_s - 0.125r_s^2 - 0.0124r_s^3 + 0.00212r_s^4 \quad (10)$$

for $r_s < 6$. It should be emphasized that $S_p(v_1, r_s)$ in our model depends on the local charge density, $\rho(\mathbf{x}) = 3/(4\pi r_s(\mathbf{x})^3)$. We note in passing that the density-functional result gives a better estimate than the linear response (dielectric) result for the stopping powers as demonstrated in the comparisons with experimental data.^{15,16} The charge density, $\rho(\mathbf{x})$, for atoms in crystal silicon in our model uses the solid-state Hartree-Fock atomic charge distribution.¹² In this approximation, there is about a one electron charge not accounted for inside the spherical muffin-tin. This small amount of charge is distributed between the maximal collision distance used in our Monte Carlo simulations and the muffin-tin radius;² within the MD scheme it provides a background charge experienced by the ion when further than the muffin-tin radius from any silicon atom.¹¹

In our simulation, the electronic stopping power is evaluated continuously along the path the ion traverses through regions of varying charge density. The energy loss is computed by

$$\Delta E_e = \int_{\text{ion path}} [Z_1 \gamma(v_1, r_s^0)]^2 S_p(v_1, r_s(x)) dx. \quad (11)$$

Finally, we discuss the difference between our approach and other electronic stopping power models used in Monte Carlo simulations based on the MARLOWE platform. There is a purely nonlocal version of the BK theory implemented into MARLOWE,¹⁷ where the effective charge and the stopping power for a proton both depend on a single nonlocal parameter, i.e., the averaged one electron radius. The energy loss for well-channeled ions in the keV region in this approach indicated that a correct density distribution is necessary to model the electronic stopping in the channel.^{17,18} Later, an implementation of a purely local version of the BK theory to model boron implants into $\langle 100 \rangle$ single-crystal silicon produced dopant profiles in good agreement with the SIMS data.¹⁹ It showed a marked improvement in modeling dopant profiles in the channel over other electronic stopping power models, such as

Lindhard and Scharff,²⁰ Firsov,²¹ and the above nonlocal implementation. However, this purely local version was unable to model the electronic stopping either for boron implants into the $\langle 110 \rangle$ axial channel, or for arsenic implants.²²

In our model, the effective charge is a nonlocal quantity, neither explicitly dependent on the impact parameter nor on the charge distribution, while the stopping power for a proton depends on the local charge density of silicon. It has been shown that it can successfully model both boron and arsenic implants into silicon over a wide range of energies and in different channeling and off-axis directions of incidence.^{2,11} In the following section, we will demonstrate that this model can be further extended to phosphorus implantation into silicon. In light of Z_1 oscillations, r_s^0 will take a slightly different numerical value from the one used in the simulations for boron and arsenic implantation.²

3. Monte Carlo and Molecular Dynamics Simulation Results

We have implemented the electronic stopping power model into the Monte Carlo simulation platform MARLOWE, which utilizes the binary collision approximation (BCA) to simulate the trajectories of energetic ions in crystalline or amorphous materials.^{23,24} For the present work, we used an extended version of MARLOWE with enhanced capabilities for modeling ion implant into silicon. This code, UT-MARLOWE,¹⁰ was selected for its more versatile features, including variance reduction for more efficient calculation, and the incorporation of important implant parameters, e.g., tilt and rotation angles, the thickness of the native oxide layers, beam divergence, and wafer temperature. The electronic stopping power model is also incorporated into an MD based implant simulator, REED.¹¹ This allows us to calculate profiles using a more realistic description of atomic collisions during implants than that provided by the BCA. It also gives us an additional verification of the model, and shows that it is independent of the simulation platform.

For the purpose of verifying the electronic stopping model, the option of the cumulative damage model in the UT-MARLOWE code was turned off in our simulations. This is a phenomenological model for estimating defect production and recombination rates. The REED cumulative damage model was also disabled. In order to minimize cumulative damage effects in the dopant profiles, simulations were performed for low to moderate dose (10^{13} cm⁻² to 3×10^{13} cm⁻²) phosphorus implants. Individual ion trajectories were simulated and the overlapping of the damage caused by different individual ion cascades was neglected. Also, use was made of 1° initial beam divergence, a 16 Å native oxide surface layer, and 300 K wafer temperature. These parameters were not cited in the experimental references but are believed to be typical for silicon doping implants.

The best suited data for verifying the electronic stopping model are the on-axis or $\langle 100 \rangle$ channeling implants. These data are highly sensitive to electronic stopping and are relatively insensitive to other effects, especially at energies of 100 keV and above where electronic stopping becomes the dominant energy loss mechanism. The free parameter in the model r_s^0 was adjusted to 1.148 Å to yield the best results in

overall comparison between the BCA and SIMS profiles. A fixed numerical value of r_s^0 was employed for all energies and directions of incidence. As commented before,² this value is physically reasonable for silicon. We note that there is only a 3.5% difference between this value of r_s^0 and the value of 1.109 Å previously used to obtain the best overall agreement with experimental data for boron and arsenic.² This difference is quite small, and our result indicates that, in general, Z_1 oscillations can be accounted for by fine-tuning of r_s^0 for a given combination of implant species and material. A slightly larger value of 1.217 Å was used for r_s^0 within the MD simulations. This difference reflects the fact that the description of ion channelling and energy loss differs between the BCA and MD schemes, and that while fitting the electronic stopping model we are also compensating for deficiencies in the implant simulation models.

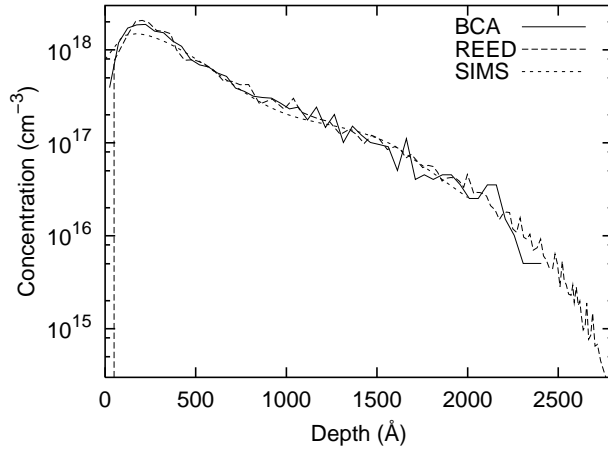


Fig. 1. Calculated and experimental dopant profiles due to 15 keV phosphorus implant for the $\langle 100 \rangle$ direction with zero tilt and rotation angles; the dose is 10^{13} cm^{-2} .

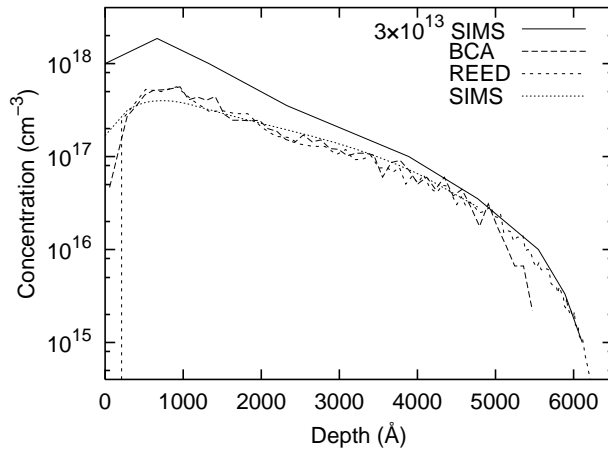


Fig. 2. Calculated and experimental dopant profiles due to 50 keV phosphorus implant for the $\langle 100 \rangle$ direction with zero tilt and rotation angles; the dose is 10^{13} cm^{-2} – the SIMS profile for a dose of $3 \times 10^{13} \text{ cm}^{-2}$ is also shown to illustrate damage effects.

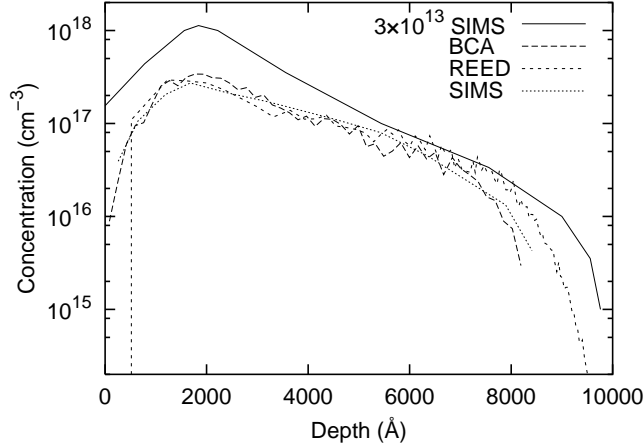


Fig. 3. Calculated and experimental dopant profiles due to 100 keV phosphorus implant for the $\langle 100 \rangle$ direction with zero tilt and rotation angles; the dose is 10^{13} cm^{-2} – the SIMS profile for a dose of $3 \times 10^{13} \text{ cm}^{-2}$ is also shown to illustrate damage effects.

We now turn to our Monte Carlo and MD dopant profile simulation results. For comparison we have digitized the SIMS data for phosphorus reported in Refs. 9 and 25. The simulated phosphorus dopant profiles are shown in comparison to the SIMS data for the channeling case in Figs. 1, 2, 3, and 4. Here, the implant energy ranges from 15 keV to 200 keV. The incidence is along the $\langle 100 \rangle$ direction with zero tilt and zero rotation angles. The dose is 10^{13} cm^{-2} or $3 \times 10^{13} \text{ cm}^{-2}$. The simulations show a close fit to the dopant distributions with depth and describe especially well the slope of the channeling tails of the dopant profiles. Some uncertainty is introduced into these comparisons by the fact that the exact implant parameters employed in the experiments are not known. Ion channeling ranges for on-axis implants may be sensitive to variations in these parameters, especially to the beam divergence. Fig. 5 illustrates the effect of changing the assumed beam divergence from 1° to 0° . As expected, the lower divergence gives a shallower slope and deeper penetration in the channeling tail. Best agreement with the SIMS profile is achieved for a divergence angle of 1° , which is quite reasonable for commercial implant machines. This value was employed in all other calculations presented here.

Another source of uncertainty is the possible influence of disorder introduced by damage to the silicon, which can reduce the average range of channeled ions. This effect was ignored in our calculations. The importance of damage can be roughly evaluated by comparing the measured SIMS profiles at different doses, as in Figs. 2 and 3. It is seen that the profiles at the higher dose are similar the lower dose profiles, but that a three-fold increase in dose results in an almost five-fold increase in dopant concentration at the peak while only doubling the concentration in the tail. However the depth of the peak and end-of-range of the profile are unaltered by the addition of damage. Hence, we can compare the ‘zero damage’ simulations to the higher dose ($3 \times 10^{13} \text{ cm}^{-2}$) SIMS data, but must be aware that the slope of the channelling tail may not match – the MD profile in Fig. 4 shows this effect.

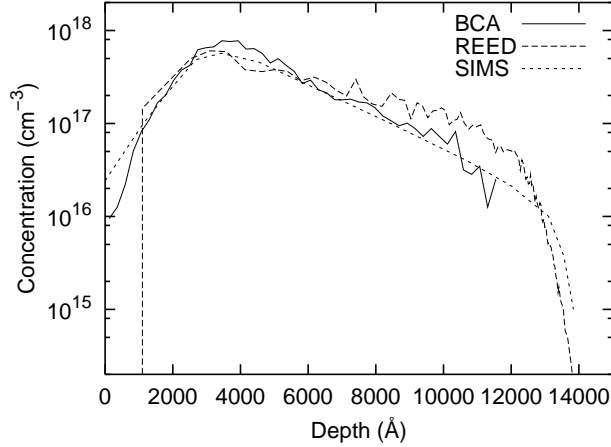


Fig. 4. Calculated and experimental dopant profiles due to 200 keV phosphorus implant for the $\langle 100 \rangle$ direction with zero tilt and rotation angles; the dose is $3 \times 10^{13} \text{ cm}^{-2}$.

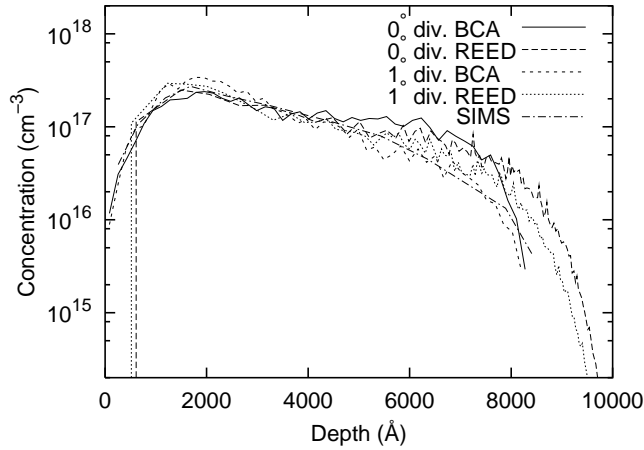


Fig. 5. Comparison of profiles calculated with 0° and 1° beam divergence; other parameters are as Fig. 3.

We conclude that the overall agreement between the simulations and experimental data for the channeling cases is excellent over a wide range of energies – especially considering that the electronic stopping model implemented in the BCA platform has been tuned by only 3.5% in the parameter, $r_s^{(0)}$.

Figs. 6 and 7 show the simulated dopant profiles in the off-axis directions, 10° tilt and 15° rotation for 100 keV, and 8° tilt and 18° rotation for 200 keV, respectively. The BCA calculated profiles show less good agreement with SIMS data than for channeling cases, with systematically deeper penetration and the concentration peak shifted by about 25% – a similar, but smaller shift is also seen for the 200 keV on-axis implant (Fig. 4).

The explanation for this discrepancy lies in the different roles of energy loss and scattering mechanisms for the off-axis implants. The average final stopping range for ions implanted in off-axis directions is controlled primarily by nuclear scattering,

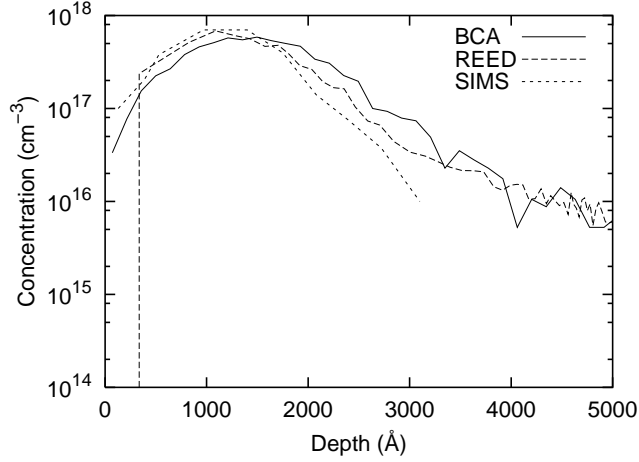


Fig. 6. Calculated and experimental dopant profiles due to 100 keV phosphorus implant for the $\langle 100 \rangle$ direction with 10° tilt and 15° rotation; the dose is 10^{13} cm^{-2} .

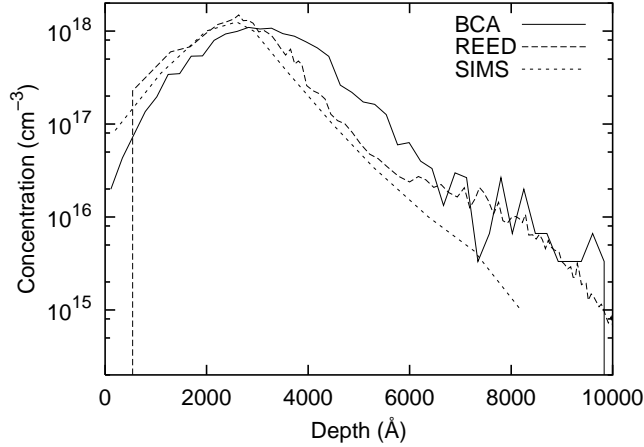


Fig. 7. Calculated and experimental dopant profiles due to 200 keV phosphorus implant for the $\langle 100 \rangle$ direction with 8° tilt and 18° rotation; the dose is $3 \times 10^{13} \text{ cm}^{-2}$.

and also by inelastic energy loss²¹ during ion-atom interactions; it is less sensitive to the electronic stopping model (except at very high energies above those investigated in this study). Accurate prediction of the off-axis profiles thus requires an accurate model for the atom-specific interatomic potential of the two species involved in the implant, plus a description of inelastic energy loss. We do not currently have an atom-specific potential model for phosphorus and silicon in the BCA platform, and there is no attempt to account for inelastic energy loss due to momentum transfer between electrons during collisions. The significance of these omissions in the BCA model was examined by performing separate calculations for random implant directions and for an implant into amorphous silicon (not shown here). These cases are completely dominated by nuclear scattering and are insensitive to electronic stopping in this energy range. The penetration ranges were too large by about 20%, verifying that nuclear scattering and inelastic energy loss are largely

responsible for the over prediction of ranges seen in the off-axis calculations.

The MD platform (REED) uses pair-specific potentials¹² for all ion-silicon interactions, and includes an inelastic energy loss model.²⁶ The off-axis profiles calculated by MD have the correct peak position and shallower penetration than the BCA profiles, and provide a better match to the SIMS data. The BCA predictions could probably be improved by the relatively simple addition of the two models mentioned above to the BCA platform, although that is outside the scope of this paper. Profiles calculated by both simulation models show an increased amount of channelling relative to the SIMS profiles. The channelling tail is due to incident ions being scattered into channelling directions in near-surface collisions. The number hard collisions near the surface due to off-axis implants will produce a significant amount of damage, even at a dose as low as 10^{13} cm⁻². Hence we should expect the ‘zero damage’ calculated profiles to show exaggerated channelling relative to the experimental data.

4. Conclusion

We have used our electronic stopping power model to simulate dopant profiles for phosphorus implantation into silicon. To account for Z_1 oscillations, we have appropriately fine-tuned the single adjustable parameter r_s^0 in our model to match the phosphorus-silicon case. The numerical value of r_s^0 is slightly greater than the one used for boron and arsenic simulations. Using this $r_s^0 = 1.148$ Å, our BCA results show excellent agreement between the simulated dopant profiles and the SIMS data over a wide range of energies for the channeling case. Less accurate but satisfactory results are obtained for off-axis implants. Detailed agreement in the off-axis direction would require additional model development for ion-silicon interactions. We have also implemented the stopping model in an MD based simulator, using a slightly larger value for r_s^0 . Using the MD implant model we achieve excellent agreement with SIMS data for both on-axis, and off-axis implants. In summary, we have successfully extended our electronic stopping power model to encompass phosphorus implantation into crystalline silicon. We have also indicated how to incorporate Z_1 oscillations with a simple phenomenological approach. We have provided a further example of implant species to verify validity of the model and to demonstrate its generality for studies of physical processes involving electronic stopping.

Acknowledgment

This work was performed at Los Alamos National Laboratory under the auspices of the U.S. Department of Energy.

References

1. J. Lindhard, M. Scharff, and H. E. Schiott, *Mat. Fys. Medd. Dan. Vid. Selsk.* **33**, 14 (1963).

2. D. Cai, N. Grønbech-Jensen, C. M. Snell, and K. M. Beardmore, *Phys. Rev. B* **54**, 17147 (1996).
3. W. Brandt and M. Kitagawa, *Phys. Rev. B* **25**, 5631 (1982).
4. N. Barberan and P.M. Echenique, *J. Phys. B* **19**, L81 (1986).
5. M. Nastasi, J. W. Mayer, and J. K. Hirvonen, *Ion-Solid Interactions: Fundamentals and Applications* (Cambridge University Press, New York, 1996).
6. P. M. Echenique, R. M. Nieminen, J. C. Ashley, and R. H. Ritchie, *Phys. Rev. A* **33**, 897 (1986).
7. F. H. Eisen, *Can. J. Phys.* **46**, 561 (1968).
8. J. S. Briggs and A. P. Pathak, *J. Phys. C* **7**, 1929 (1974).
9. R. G. Wilson, *J. Appl. Phys.* **60**, 2797 (1986).
10. S. H. Yang, S. Morris, S. Tian, K. Parab, M. Morris, B. Obradovich, C. M. Snell, and A. F. Tasch, *UT-MARLOWE Version 3.0*, (Microelectronics Research Center, The University of Texas at Austin, 1995).
11. K. M. Beardmore and N. Grønbech-Jensen, *Phys. Rev. E* **57**, in press (1998).
12. J. F. Ziegler, J. P. Biersack, and U. Littmark, *The Stopping and Range of Ions in Solids* (Pergamon Press, New York, 1985).
13. S. Kreussler, C. Varelas, and W. Brandt, *Phys. Rev. B* **23**, 82 (1981).
14. P. M. Echenique, R. M. Nieminen, and R. H. Ritchie, *Solid State Commun.* **37**, 779 (1981).
15. A. Mann and W. Brandt, *Phys. Rev. B* **24**, 4999 (1981).
16. W. Brandt, *Nucl. Instrum. Methods* **194**, 13 (1982).
17. N. Azziz, K. W. Brannon, and G. R. Srinivasen, in *Ion Beam Processes in Advanced Electronic Materials and Device Technology – MRS Symp. Proc. No. 45*, ed. B. R. Appleton, F. H. Eisen, and T. W. Sigmon (Materials Research Society, Pittsburgh, 1985), p. 71.
18. C. S. Murthy and G. R. Srinivasen, *IEEE Trans. Electron. Devices*, **39**, 264 (1992).
19. K. M. Klein, C. Park, and A. F. Tasch, *IEEE Trans. Electron. Devices* **39**, 1614 (1992).
20. J. Lindhard and M. Scharff, *Phys. Rev.* **124**, 128 (1961).
21. O. B. Firsov, *Zh. Eksp. Teor. Fiz* **36**, 1517 (1959) [*Sov. Phys. JETP* **36**, 1076 (1959)].
22. S. H. Yang, S. J. Morris, S. Y. Tian, K. B. Parab, and A. F. Tasch, *IEEE Trans. Semicond. Manufacturing* **9**, 49 (1996).
23. M. T. Robinson and I. M. Torrens, *Phys. Rev. B* **9**, 5008 (1974).
24. W. Eckstein, *Computer Simulation of Ion-Solid Interactions* (Springer-Verlag, New York, 1991).
25. R. J. Schreutelkamp, V. Raineri, F. W. Saris, R. E. Kaim, J. F. M. Westendorp, P. F. H. M. van der Meulen, and K. T. F. Janssen, *Nucl. Instrum. Methods Phys. Res. Sect. B* **55**, 615 (1991).
26. L. M. Kishinevskii, *Izv. Acad. Nauk. SSSR, ser. fiz.* **26**, 1410 (1962); V. A. Elteckov, D. S. Karpuzov, Yu. V. Martynenko, and V. E. Yurasova, in *Atomic Collision Phenomena in Solids*, ed. D. W. Palmer, M. W. Thompson, and P. D. Townsend (North Holland, Amsterdam, 1970), p. 657.